






Letter

Mapping Paddy Rice Using Sentinel-1 SAR Time Series in Camargue, France

Hassan Bazzi ^{1,*}, Nicolas Baghdadi ¹, Mohammad El Hajj ¹, Mehrez Zribi ²,
Dinh Ho Tong Minh ¹, Emile Ndikumana ¹, Dominique Courault ³ and Hatem Belhouichette ⁴

¹ IRSTEA, TETIS, University of Montpellier, 500 rue François Breton, 34093 Montpellier CEDEX 5, France; nicolas.baghdadi@teledetection.fr (N.B.); mohammad.el-hajj@teledetection.fr (M.E.H.); dinh.ho-tong-minh@irstea.fr (D.H.T.M.); emile.ndikumana@irstea.fr (E.N.)

² CESBIO (CNRS/UPS/IRD/CNES), 18 av. Edouard Belin, bpi 2801, 31401 Toulouse CEDEX 9, France; mehrez.zribi@ird.fr

³ UMR 1114 EMMAH, INRA, University of Avignon, 84914 Avignon, France; dominique.courault@inra.fr

⁴ CIHEAM-IAMM, UMR-System, 34090 Montpellier, France; belhouichette@iamm.fr

* Correspondence: hassan.bazzi@irstea.fr; Tel.: +33-4-6704-6300

Received: 14 January 2019; Accepted: 9 April 2019; Published: 11 April 2019



Abstract: This study proposes an effective method to map rice crops using the Sentinel-1 SAR (Synthetic Aperture Radar) time series over the Camargue region, Southern France. First, the temporal behavior of the SAR backscattering coefficient over 832 plots containing different crop types was analyzed. Through this analysis, the rice cultivation was identified using metrics derived from the Gaussian profile of the VV/VH time series (3 metrics), the variance of the VV/VH time series (one metric), and the slope of the linear regression of the VH time series (one metric). Using the derived metrics, rice plots were mapped through two different approaches: decision tree and Random Forest (RF). To validate the accuracy of each approach, the classified rice map was compared to the available national data. Similar high overall accuracy was obtained using both approaches. The overall accuracy obtained using a simple decision tree reached 96.3%, whereas an overall accuracy of 96.6% was obtained using the RF classifier. The approach, therefore, provides a simple yet precise and powerful tool to map paddy rice areas.

Keywords: rice; SAR; Sentinel-1; random forest; decision tree; classification

1. Introduction

Rice is a staple food resource for more than half of the world population. It plays an important role in the global economy, food security, and water use. In 2017, rice was classified by the FAO (Food and Agriculture Organization of the United Nations) as the second most produced cereal in the world [1]. Moreover, according to the International Food Policy Research Institute, the demand for rice is increasing by 1.8% per year. Thus, obtaining information on the rice's location and distribution is of great importance for food security and water use.

Considered as an important reservoir of biodiversity, the Camargue region of South France is the main producer and supplier of rice in France. Rice in Camargue plays an important role in the hydrological balance of the region [2]. In fact, rice crops prevent high levels of salinity in the low lying soils and thus offer a temporary habitat to migratory bird species. Additionally, rice production in the region has a significant impact on the regional economy. Therefore, mapping the spatial extent of the rice is of great importance for the agriculture sector in France.

Several studies have reported using remote sensing for land surface monitoring in agricultural areas [3–8]. This is particularly the case for rice mapping. Among the many optical sensors, MODIS,

Landsat, and most recently Sentinel-2 have been used to map irrigated paddy rice [9–12]. For example, Xiao et al. [9] used the time series of MODIS-derived vegetation indices (LSWI: Land Surface Water Index, EVI: Enhanced Vegetation Index, and NDVI: Normalized Differential Vegetation Index) to map paddy rice during the phases of flooding and transplanting. Their study was based on the unique spectral reflectance of the flooded soil-vegetation mix compared to other croplands. Additionally, Clauss et al. [13] mapped rice areas in China using MODIS time series products and the support vector machine. The overall accuracy achieved was 0.90 with a kappa coefficient of 0.77. Moreover, Li et al. [14] developed a phenology-based algorithm to map rice areas over the Poyang Lake Plain, China using the normalized EVI and SAVI (Soil Adjusted Vegetation Index) derived from Landsat-8 images. They achieved an overall accuracy of 96.8% and a correlation coefficient $R^2 = 0.88$ when comparing the produced map with national statistics. However, the cloud cover limits the use of high spatial resolution optical images for rice mapping, especially in tropical areas where there is cloud cover more than 70% of the time during the rice growing season. On the other hand, several studies investigated the capabilities of SAR (Synthetic Aperture Radar) data for rice mapping and monitoring. These studies assessed the potential of SAR data in the L-band [15], C-band [16,17], and X-band [18] for rice monitoring. In many studies, rice fields have been mapped based on the low radar backscattering signal of rice plots in the beginning of the season when the fields are flooded [19–21]. Other studies used the temporal behavior of the radar backscattering signal in several polarizations to map paddy rice [22–24]. Lasko et al. [24] used random forest classification to map rice areas using a time series of Sentinel-1 SAR images in Hanoi, Vietnam. In their study, the highest overall accuracy ($93.5\% \pm 1.33$) was achieved using the ratio of the VV and VH polarizations. Moreover, Forino et al. [23] used the ratio of the HH and VV polarizations derived from the Cosmo Sky-Med SAR data to map rice areas in the Mekong Delta, Vietnam. Recently, Ndikumana et al. [25] applied a deep recurrent neural network (DNN) on a Sentinel-1 SAR time series to classify the agricultural land cover in Camargue, France. They reached an overall accuracy of 89.6% for agricultural classification.

The recently launched Sentinel-1 SAR satellite offers a powerful tool for agricultural area classification and monitoring under various weather conditions. The Sentinel-1 satellites provide an exceptional combination of high spatial and high temporal resolutions for dual polarization synthetic aperture radar data (6 days of temporal resolution and a $10\text{ m} \times 10\text{ m}$ pixel spacing). The availability of a dense time series enables the derivation and analysis of temporally backscattered signals.

This study concentrates on the use of Sentinel-1 temporal backscatter signatures of rice cultivation to accurately map rice areas. We present a new approach for mapping rice areas using a Sentinel-1 SAR time series over the Camargue region of south-east France. First, the temporal behavior of SAR backscattering derived from Sentinel-1 images was analyzed over all existing crop types. Then, we took advantage of the exclusive temporal profile of the rice crop in VH polarization and the VV/VH ratio, compared to other crop types in the area, to identify a rice plot. Numerous metrics were derived using the Gaussian fitting of the VV/VH ratio and the linear fitting of the VH time series that were found to best discriminate rice crops from other crop types. Finally, we applied a decisional tree and a Random Forest (RF) classifier using the derived metrics to map the rice areas in the Camargue region. After a detailed description of the study site and dataset in Section 2, Section 3 presents the proposed methodology. The results and validation are presented in Section 4. A discussion is presented in Section 5 and finally Section 6 presents the main conclusions.

2. Materials

2.1. Study Site

The study site is the Camargue region located in the south-east of France (centered on $4^{\circ}35'$ E and $43^{\circ}33'$ N) (Figure 1). The Camargue has a Mediterranean climate with a mild winter and a long dry summer. It has a variety of landscapes, such as agricultural areas, urban zones, water areas, and forests. Agriculture is the main economic sector of the Camargue region. However, among agricultural crops

rice is the most dominant crop type, having an important impact on the economy and ecology of the region. According to the INRA (National Institute of Agricultural Research) data of 2011, rice crop in the Camargue comprises 55% of the agricultural crops. Rice in Camargue is frequently grown in rotation with rain-fed crops, especially wheat, depending on the soil types. For deep soils, rice is frequently replaced by durum wheat and is cultivated for one to five years. For shallow soils, farmers usually prefer continuous rice cultivation [2].

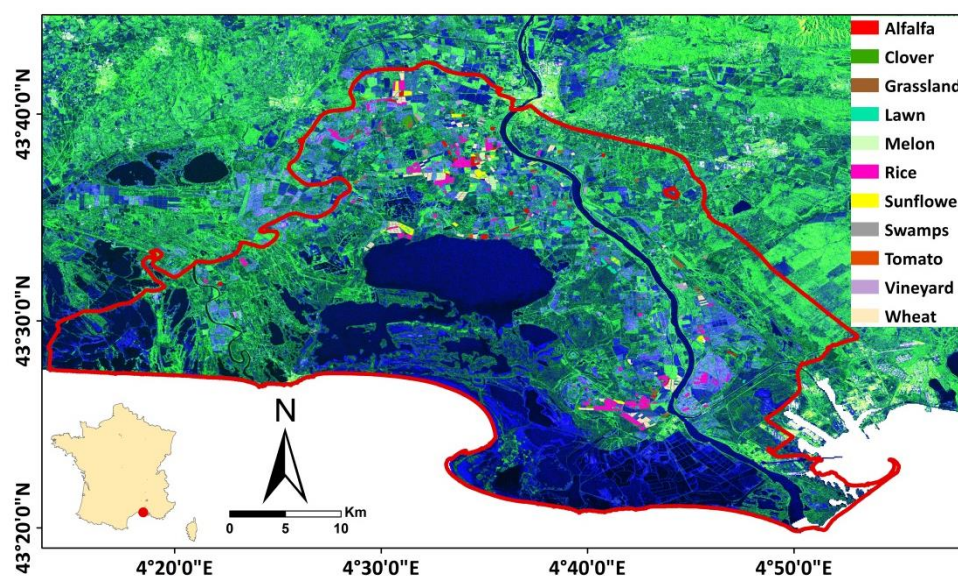


Figure 1. Location of the study site, Camargue, France. The red border represents the study area and the colored polygons represent the reference parcels. The background is a SAR) composite of three bands (Red: VV, Green: VH, and Blue: VV/VH).

2.2. Ground Data

The land cover of 832 reference plots were collected during a field survey performed in July 2017 [25]. The observed crop types are: Alfalfa, Clover, Grassland, Lawn, Melon, Rice, Sunflower, Swamps, Tomato, Vineyards, and Wheat (Figure 1). Table 1 summarizes the number of plots for each type. The crop type classification of 2017 performed by Ndikumana et al. [25] revealed that the agricultural area of the Camargue region is mostly occupied by rice, covering 29.3% of the total agricultural area. The second most important crop observed is winter wheat with 20.5%. Additionally, both lawn and grassland occupy 20% of the total crop area.

Table 1. Distribution of the reference plots per class of land cover.

Crop Type	Number of Plots	Surface Area (ha)
Alfalfa	45	139
Clover	26	76
Grassland	49	157
Lawn	27	201
Melon	23	76
Rice	319	1072
Sunflower	78	230
Swamps	19	101
Tomato	14	48
Vineyards	28	119
Wheat	204	650
Total	832	2869

Figure 2 shows the temporal variation of the Normalized Differential Vegetation index (NDVI) for each crop type between March and October 2017. These NDVI values are calculated using Sentinel-2 images corrected for atmospheric effects and averaged for each crop type. Among the observed crop types, wheat is the only winter crop in the region. Additionally, it can be noticed that Camargue has a single cropping season of rice. According to the performed field surveys, the sowing of the rice crop in 2017 occurred in the first 15 days of May and the harvesting occurred from the end of September to the beginning of October.

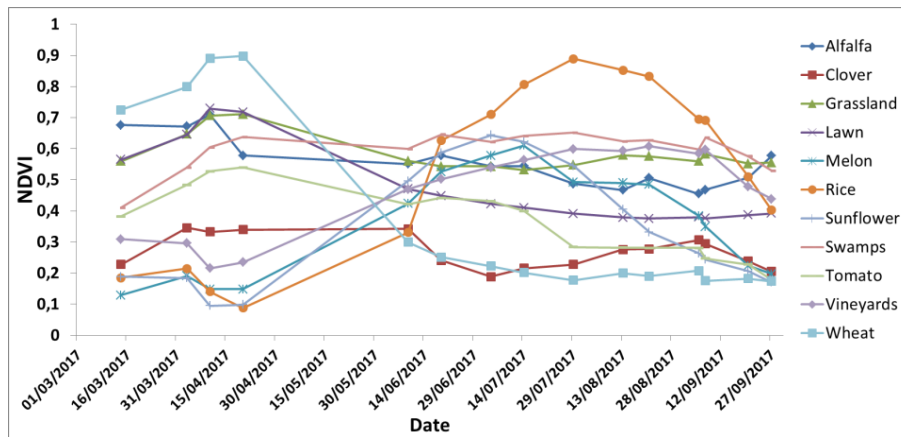


Figure 2. NDVI time series of 11 crop types in the study area.

2.3. SAR Data

Since rice cultivation in Camargue takes place between May and October of each year, we focus our analysis of SAR data only on this period. For this reason, thirty-one S1 images obtained from the Sentinel-1A (S1A) and Sentinel-1B (S1B) satellite constellation operating at the C-band (frequency = 5.406 GHz, wavelength ~ 6 cm) were downloaded for the period between 08 April 2017 and 29 October 2017. The 31 S1 images used were acquired in the Interferometric Wide Swath (IW) imaging mode with the VV and VH polarizations. In addition, the images were generated from the high-resolution Level-1 Ground Range Detected (GRD) product with 10 m × 10 m pixel spacing. These Sentinel-1 images are available via the Copernicus website (<https://scihub.copernicus.eu/dhus/#/home>). To calibrate the S1 images (radiometric and geometric correction); the Sentinel-1 Toolbox (S1TBX) developed by the ESA (European Spatial Agency) was used. The radiometric calibration aims to convert the digital number values of the S1 images into backscattering coefficients (σ^0) in a linear unit. The radiometric accuracy of the Sentinel-1 SAR backscattering coefficient is approximately 0.70 dB (3σ) for the VV polarization and 1.0 dB (3σ) for the VH polarization [26]. The aim of the geometric correction is to ortho-rectify the S1 images using the digital elevation model of the SRTM “Shuttle Radar Topography Mission” at 30 m spatial resolution. It is good to mention here that the study area is relatively flat with no high slope areas. A multi-temporal speckle filter, given in Equation (1), was then applied to the 31 calibrated S1 images to reduce the speckle noise in each SAR image [27]. Finally, a temporal series of 31 calibrated S1 images were obtained in the WGS-84 geographic coordinate system (World Geographic System 1984).

$$J_k(x, y) = \frac{\langle I_k(x, y) \rangle}{M} \sum_{i=1}^M \frac{I_i(x, y)}{\langle I_i(x, y) \rangle} \quad (1)$$

where $J_k(x, y)$ is the radar intensity of output image k at pixel (x, y) , $I_i(x, y)$ is the radar intensity of input image i at pixel (x, y) , and $\langle I_i(x, y) \rangle$ is the local mean intensity of input image I at pixel (x, y) .

3. Methodology

A comprehensive overview of the methodology is presented in Figure 3. First, the temporal behavior of the Sentinel-1 SAR backscattering coefficients (σ°) over agricultural plots was studied to determine the best metrics that identify and discriminate the rice plots. Two methods were tested for mapping the rice areas. The first used the decision tree and the second was based on a Random Forest classifier. For the plots' limit, we used a thematic vector file of land cover produced by INRA in 2011. First, agriculture plots were extracted by masking the urban, water and forest plots. The extracted plots contain the 832 reference plots surveyed for crop types in 2017 (described in Section 2.2). Then, the mean backscattering coefficient was calculated for each plot from each preprocessed S1 image by averaging the σ° values in the linear unit of all the pixels within the plot. The mean values of the 832 reference plots were further used for analyzing the temporal behavior of SAR backscattering and generating the suitable metrics used for classification.

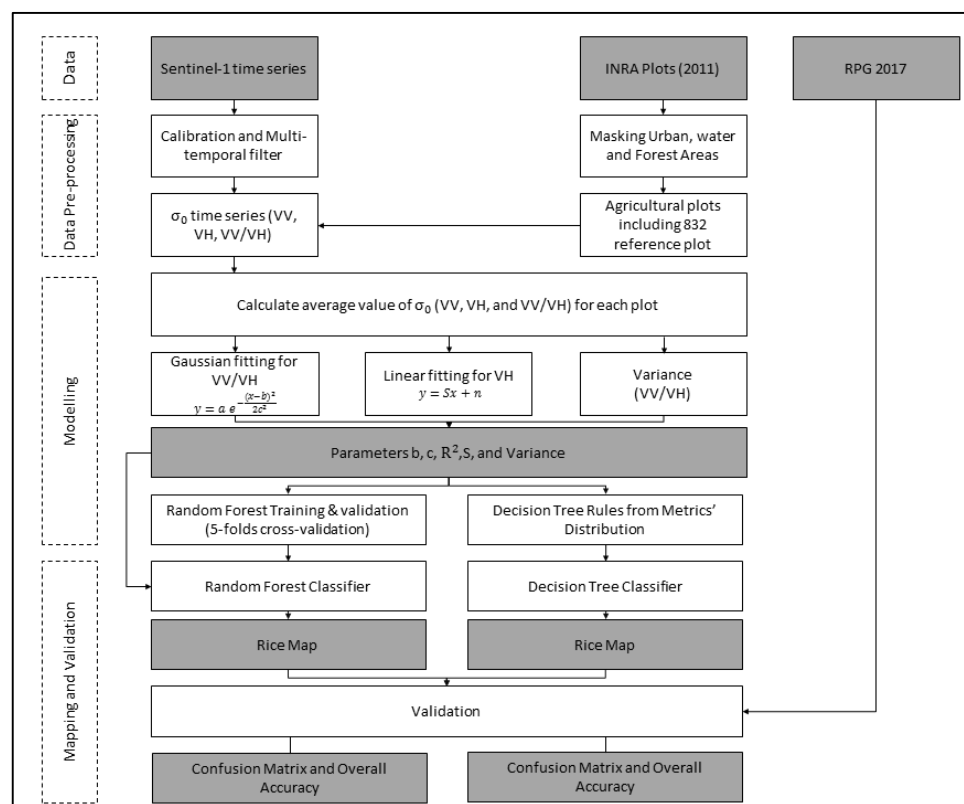


Figure 3. Workflow overview using a decision tree and Random Forest (RF) classifier.

3.1. Temporal Behavior of σ° SAR Backscattering over Agricultural Plots

An analysis of the temporal behavior of the Sentinel-1 backscattering coefficient σ° at the VV and VH polarizations as well as the ratio of VV/VH was performed over all the crop types of the reference plots to define the metrics that allow the separation of the rice plots. Figures 4 and 5 show the backscattering coefficient σ° averaged for all reference plots of the same crop type at each date and plotted with the corresponding standard deviation. By comparing the temporal behavior of the time series signals for rice with that of each crop type, we observe that the rice plots have a different temporal behavior for both the VV/VH ratio and VH backscattering. In fact, the temporal series of the VV/VH signal for rice approximately follows a Gaussian behavior for the period between May and September (Day of Year (DOY) between 120 and 270) (Figure 5). Moreover for the VH signal, the rice shows an increasing linear profile during the same period. In addition, VV/VH shows a high variance for rice. These unique characteristics of rice are used to classify the rice cultivated plots.

The calculated metrics, used for classification, includes the Gaussian fitting parameters of the VV/VH time series, the variance of the VV/VH signal, and the slope of the linear fitting of the VH signal (between May-DOY 120 and September-DOY 270).

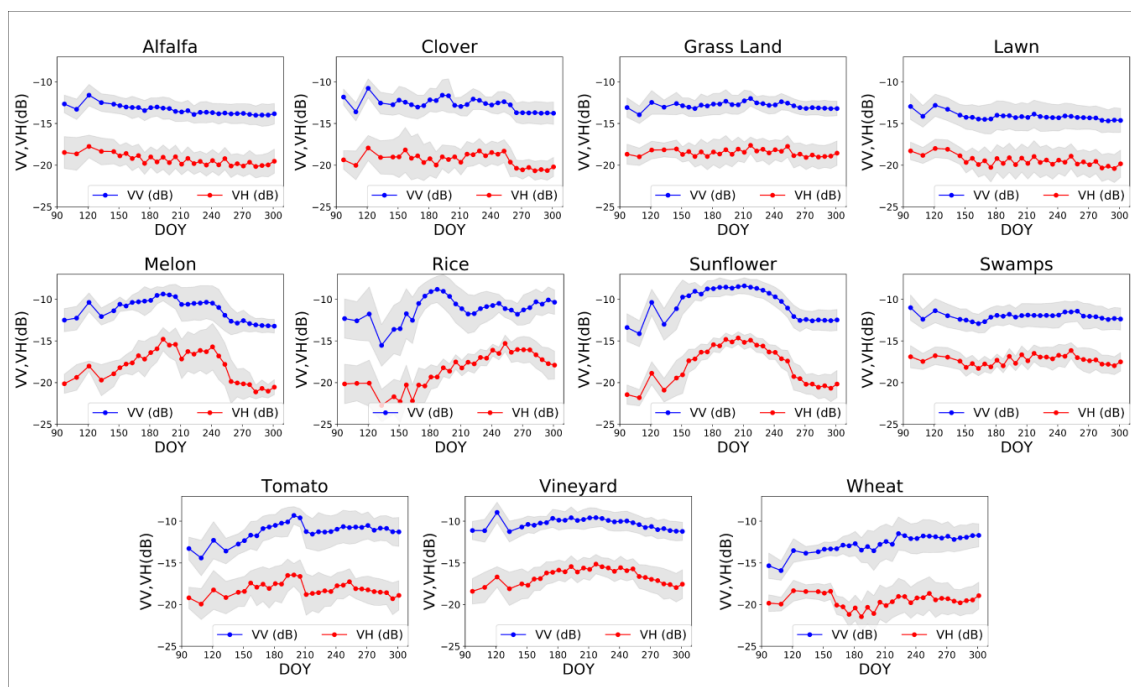


Figure 4. Temporal evolution of SAR backscattering coefficient σ^o of 11 crop types for VV and VH polarizations. Mean values are represented by dots and standard deviations are represented by the filled color domains surrounding the curves.

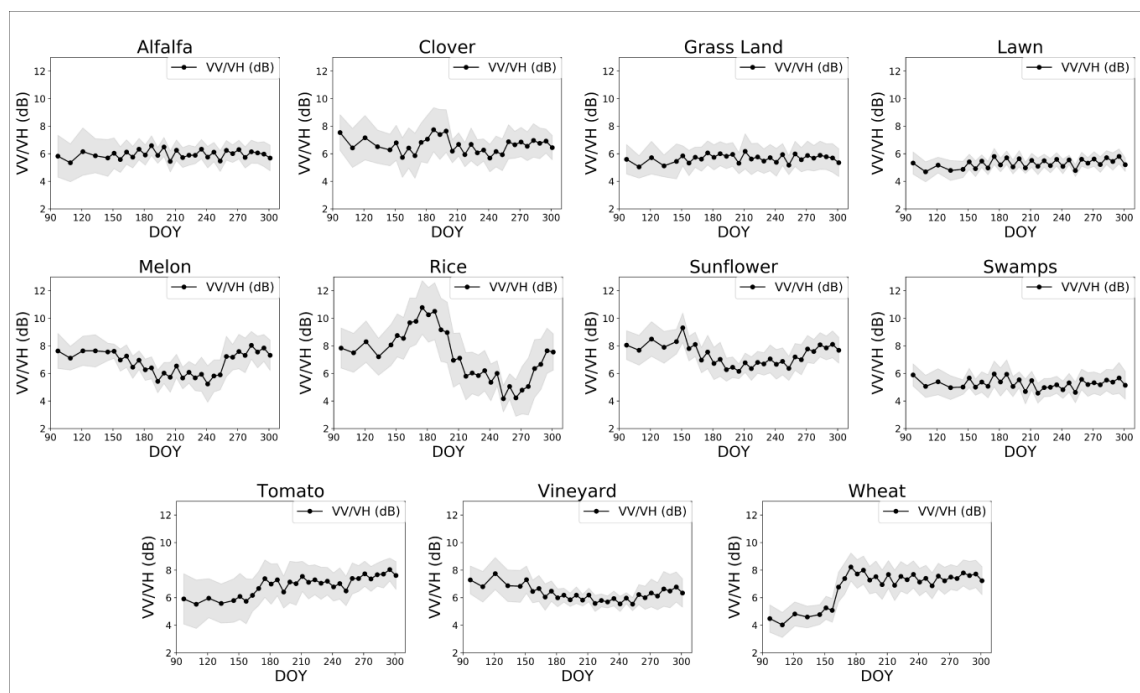


Figure 5. Temporal evolution of the ratio VV/VH for SAR backscattering coefficient σ^o of 11 crop types. Mean values are represented by dots and standard deviations are represented by the filled color domains surrounding the curves.

3.1.1. Gaussian Fitting of VV/VH

The profile of the time series for VV/VH follows a Gaussian bell shape for the rice plots. This characteristic is especially observed over rice cultivation. For this reason, we proposed fitting the VV/VH time series of each plot with a Gaussian function. First, the time series values of VV/VH for each reference plot were normalized using the unity-based normalization in Equation 2 to adjust the values at a common scale (between 0 and 1).

$$Y' = \frac{Y - Y_{\min}}{Y_{\max} - Y_{\min}} \quad (2)$$

where Y' is the normalized value, Y is the initial value of the time series, Y_{\min} is the minimum value of the time series, and Y_{\max} is the maximum value of the time series.

To avoid small and noisy peaks of the raw VV/VH data (black curve in Figure 6), the temporal series of the VV/VH ratio was smoothed for each reference plot using a Gaussian filter (blue curve in Figure 5). The smoothed data allowed us to estimate the peak position and amplitude required to initialize the Gaussian fitting. In fact, the Gaussian fitting with the least square method requires the initial values of the peak position and amplitude. Using the least square method, the VV/VH time series was then fitted with a Gaussian function presented in Equation 3 (red curve in Figure 6):

$$y = a e^{-\frac{(x-b)^2}{2c^2}} \quad (3)$$

where a is the amplitude, b is the position of the maximum in days, and c is the standard deviation of the fitting function in days.

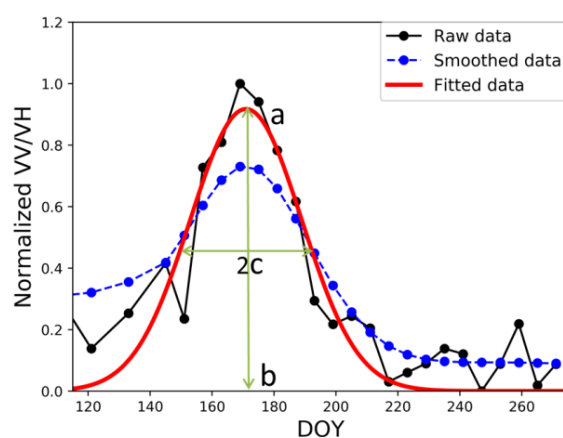


Figure 6. Gaussian fitting of the VV/VH temporal series for a rice plot with the corresponding fitting parameters. Raw normalized data in black, smoothed data in blue and Gaussian fitted data in red.

For each plot we can then obtain the resultant fitting parameters a , b , and c , as well as the correlation coefficient R^2 . Since the rice crop is the only crop among the 11 studied crops that follows the Gaussian profile in VV/VH ratio, it is possible to distinguish the rice plots using the obtained fitting parameters.

3.1.2. VV/VH Signal Variance

Variance is the expectation of the squared deviation of a random variable from its mean. Informally, it measures how far a set of numbers is spread out from their average value. It is expected that the variance values for VV/VH in rice plots are higher than other crop types, since the values change rapidly during the growing season. For example, Figure 4 shows a slight variation of VV/VH for vineyards, grasslands, and swamps during the period between May and September, whereas an important variation of the VV/VH signal is observed for the rice plots. For this reason, the variance value of

VV/VH was calculated for each parcel and is considered to be an additional metric for classifying rice plots.

3.1.3. VH Linear Fitting

Another unique observation for rice cultivation is the increasing linear profile of the VH backscattering during the growing cycle (between DOY 120 and 270). Thus, the VH temporal series of each plot was fitted with a linear regression model according to Equation 4:

$$y = Sx + n \quad (4)$$

Therefore, for each plot we can obtain the resultant slope (S in dB/DOY) and intercept (n). Rice crops can be thus discriminated using high positive slope values of the fitted linear model compared to other crop types.

3.2. Decision Tree Classification

To classify rice crops, a decision tree based on four extracted metrics was built. The rules of the decision tree were determined from the distribution of the values of metrics for all crop types (Figure 7). The results show that a plot with rice cultivation can be identified using the following rules:

$$Rice = \begin{cases} 140 \leq b \leq 210 \\ R^2 \geq 0.5 \\ \text{Variance} \left(\frac{VV}{VH} \right) \geq 2.5 \\ S > 0.01 \end{cases} \quad (5)$$

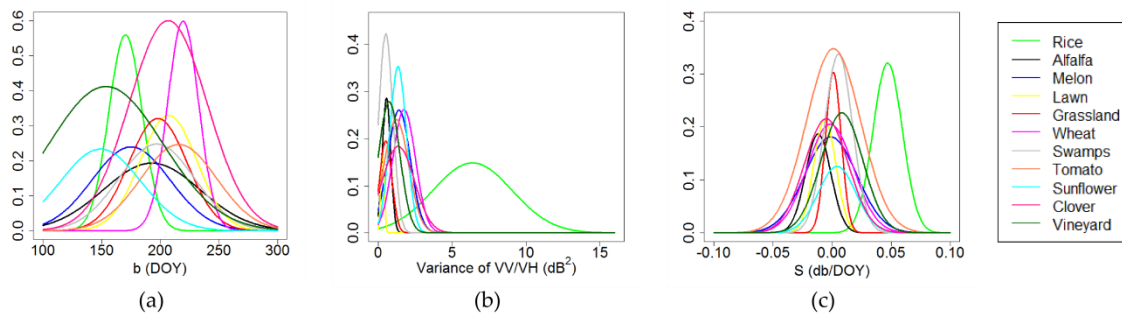


Figure 7. Distribution of the (a) position of the maximum of the VV/VH Gaussian fitting; (b) variance of the VV/VH time series; and (c) slope of the VH linear fitting for 11 crop types represented by the normal distribution function.

The values of b and R^2 are related to the Gaussian fitting of VV/VH because the temporal series of VV/VH follows a Gaussian function for rice, thus the fitting values of b and R^2 are within the proposed thresholds. The R^2 of the Gaussian fitting was higher than 0.5 for rice and lower than 0.5 for all other crop types. The condition on S represents the increasing linear profile of the rice cultivation in VH polarization. A lower limit value of 0.01 for S was proposed to describe this increasing linear profile. In addition, a lower limit of 2.5 on the variance of the (VV/VH) time series determines whether the signal has an important variation, which corresponds only to rice cultivation. The accuracy of the proposed decision tree classification is further presented in Section 4.

3.3. Random Forest Classification

Random Forests (RF) is a learning method for classification based on generating a large number of decision trees, where each is constructed using a different subset of the training set. These subsets are usually selected by sampling at random and with replacement from the original data set. The decision

trees are then used to identify a classification consensus by selecting the most common output. It has demonstrated its ability to yield high quality classification with a high computational time. In our study, we classified rice and non-rice plots by introducing the extracted metrics into the random forest classifier available via the “R” open statistical computing software (Package “randomForest”). The random forest is trained using the values of the position of the maximum (b), the standard deviation (c), and the correlation coefficient (R^2) of the VV/VH Gaussian fitting, the variance of VV/VH, and the slope S of the VH linear fitting for the 832 reference plots for the two classes (Rice and other crops). In fact, 5 folds cross-validation is first performed using the 832 reference plot. To do so, the dataset is randomly divided into 5 folds of equal size. Four folds are used to train the model, and the fifth fold is used for the validation phase. This operation is repeated five times, so that each fold will be a possible validation set. The number of trees chosen is 300 and the number of features used in the construction of each tree is 2. Finally, the map obtained using the trained RF classifier was further compared to the available national data. The overall accuracy, Kappa, and F_1 score were calculated for the obtained confusion matrix [28,29]:

$$\text{Overall Accuracy "P}_0\text{"} = \frac{TP + TN}{TP + TN + FN + FP} \quad (6)$$

$$\text{Expected Accuracy "P}_e\text{"} = \frac{(TP + FP) \times (TP + FN) + (FN + TN) \times (FP + TN)}{(TP + TN + FN + FP)^2} \quad (7)$$

$$\text{Kappa} = \frac{P_0 - P_e}{1 - P_e} \quad (8)$$

$$F_1 \text{ score} = \frac{2TP}{2TP + FP + FN} \quad (9)$$

where TP is the number of the rice plots truly classified as rice plots, TN is the number non-rice plots truly classified as non-rice plots, FP is the number of non-rice plots falsely classified as rice, FN is the number of rice plots falsely classified as non-rice plots, N is the total number of plots, P_0 is the observed accuracy and P_e is the expected accuracy.

4. Results

In this section, we report the results of the proposed classifications. First, the 5 folds cross-validation of the RF classifier shows that out of the 319 rice plots only 5 plots were miss-classified as other crops and one non-rice plot was classified as rice. The confusion matrix obtained when performing the 5 folds cross-validation shows an overall accuracy of 99.2%. Then, the performance of the proposed classifications (decision tree and random forest) was assessed by comparing the produced rice map to the national data of the RPG-2017 (Graphical Registered Parcels) provided freely by the French government (<https://www.data.gouv.fr>). The validation is done over all of the classified plots in our study area (9976 plots in total). Each field is checked if it is correctly classified through being compared with the declared rice plots of the RPG data. Table 2 shows the confusion matrix obtained using the simple decision tree, whereas Table 3 presents the confusion matrix produced using the random forest classification. The overall accuracy, Kappa, and F_1 score for both classifiers were calculated. Similar high accuracy is obtained using both proposed methods. The RF classifier produces an overall accuracy of 96.7% whereas the decision tree gives 96.3% overall accuracy. In fact, using the proposed decision tree, 325 rice plots were misclassified as non-rice plots, whereas using the RF classifier 266 rice plots were misclassified as non-rice plot according to the RPG data. Additionally, using the RF classifier 68 non-rice plots were classified as rice, whereas using the decision tree method 47 non-rice plots were classified as rice.

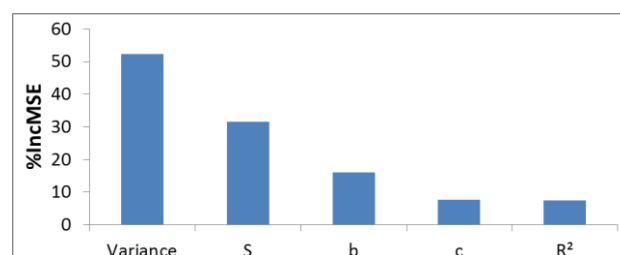
Table 2. Confusion matrix for decisional tree classification.

Class Value	Rice	Other Crop	Total	User Accuracy
Rice	3120	325	3445	90.5%
Other Crop	47	6475	6522	99.2%
Total	3167	6800	9967	
Producer Accuracy	98.5%	95.2%		
Overall Accuracy			96.3%	
Kappa			91.5%	
F ₁ score			94.3%	

Table 3. Confusion matrix for the RF classifier.

Class Value	Rice	Other Crop	Total	User Accuracy
Rice	3179	266	3445	92.3%
Other Crop	68	6454	6522	98.9%
Total	3247	6720	9967	
Producer Accuracy	97.9%	96.0%		
Overall Accuracy			96.6%	
Kappa			92.5%	
F ₁ score			95.0%	

Moreover, the metrics' importance was assessed for the random forest classifier. The significant metrics that contributed the most to the classification of the rice plots were analyzed according to the increase in the mean square error (%IncMSE) of the predictions (Figure 8). The results show that the high significant metrics are the variance of the VV/VH and the slope of the linear fitting of the VH, whereas the less significant metrics are the maximum position and standard deviation of the Gaussian fitting of VV/VH.

**Figure 8.** Metrics' order of importance in the RF classifier.

The rice area map of the Camargue region was finally established by applying the generated random forest classifier (Figure 9a). The estimated rice area in 2017 obtained using the proposed classification is 9740 ha. Comparing this area to the rice area from the IGN data of 2011, we observe that the rice cultivation area has significantly decreased in the region from 16,000 ha in 2011 to 9740 ha in 2017 (our estimation). The obtained rice area was then compared to the rice area declared in the RPG data (Figure 9b). Using the proposed classification the rice area was estimated as 9740 ha slightly lower than the declared area (10,015 ha). Thus, the overall accuracy in the rice area estimation reaches 97.3%. According to the proposed classification, the rice area in 2017 occupied approximately 32.5% of the total agricultural area. This percentage of rice crops agrees with the percentage obtained by Ndikoumana et al. [25] (29.3%).

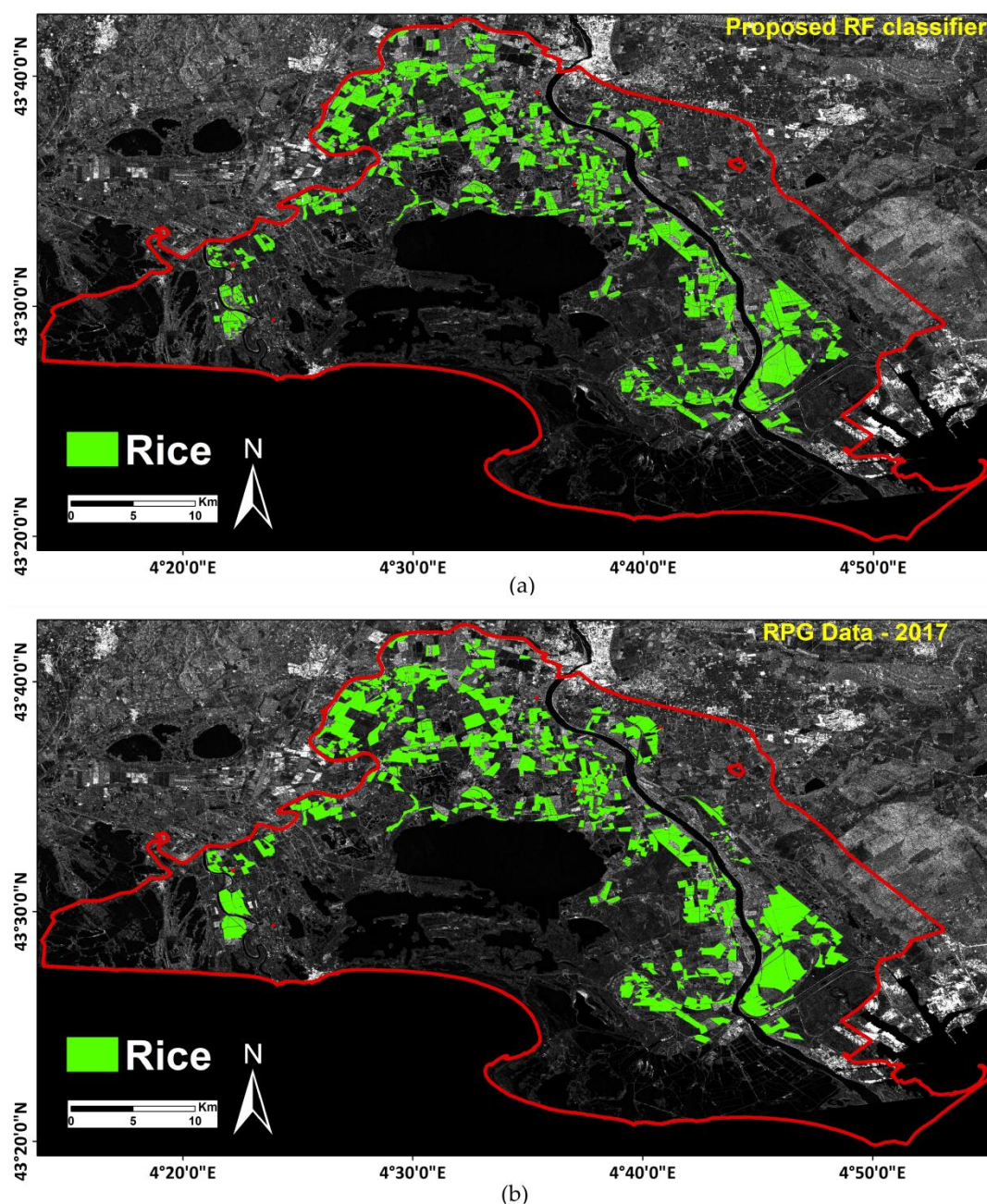


Figure 9. (a) Rice areas in Camargue in 2017 using our proposed RF classifier, (b) Rice areas in Camargue in 2017 declared by the RPG-2017. The background in both maps is a SAR image in VV polarization.

5. Discussion

In this study we mapped rice areas in the Camargue region using Sentinel-1 SAR backscattering time series and two classification approaches: random forest and decision tree. We first analyzed the SAR backscattering coefficient over the entire agricultural crop existing in the area and showed that the rice plots have a specific temporal profile in VH polarization and in the VV/VH ratio. Then, we mapped then rice areas based on metrics derived from the VH and VV/VH time series. The obtained results were finally compared to existing national data. This validation indicated that the proposed approach has good performance where the overall accuracy was 96.6% and Kappa coefficient was better than 92.5% (using RF classifier).

To properly assess the quality of the obtained results, we compared the classification results with results obtained by other classification methods using the same dataset. Through literature,

Ndikumana et al. [25] classified the agricultural areas in Camargue, France by applying the deep recurrent neural network (DNN) on a Sentinel-1 SAR time series. Rice crop was one of the classified agricultural crops. They showed that the overall accuracy of the agricultural classification using the DNN is 89.6%. In particular, the confusion matrix obtained using the 5 folds cross-validation of the DNN showed that the producer accuracy of the rice class reaches 95.7% and the user accuracy reaches 97.5%. In their study, they also tested the RF classifier using the S1 time series. The confusion matrix obtained using the RF classifier shows that the producer accuracy for rice class reached 92.7% and the user accuracy reached 97.6% when performing the 5 folds cross-validation. On the other hand, the 5 folds cross-validation of the RF classifier in our approach shows that the producer accuracy reaches 99.0% while the user accuracy reaches 98.4%. Figure 10 presents the classified rice areas produced using their proposed approach (using the DNN). Since their approach uses the same dataset as our study (Sentinel-1 time series and ground data) and was accomplished for the same year (2017), a comparison was also performed between the obtained rice class of Ndikumana et al. [25] and the RPG-2017. The 9976 plots classified in our proposed approach were checked for being rice or other crop in the agricultural land cover map proposed by Ndikumana et al. [25] and then compared to the previous results obtained for RPG data. Table 4 presents the confusion matrix produced by comparing Ndikumana's rice areas and RPG rice areas based on the classified plots in our approach. The overall accuracy of the Ndikumana rice classification when compared to RPG is 94.4% slightly lower than the accuracy obtained using our approach (96.6%). Both the user and producer accuracies are higher for our approach (92.3% and 97.9% respectively) compared to Ndikumana's approach (88.3% and 95.2% respectively) when comparing to the RPG data. Based on the comparison of both rice areas to the RPG data, we can conclude that our proposed method remains a powerful tool to map paddy rice areas. The complexity of the method used by Ndikumana et al. [25] to produce the land cover map and the simplicity of our method with better accuracy makes our proposed approach powerful for rice area mapping. However, it is good to mention that Ndikumana et al. [25] classified the 11 agricultural classes, rather than only the paddy rice.

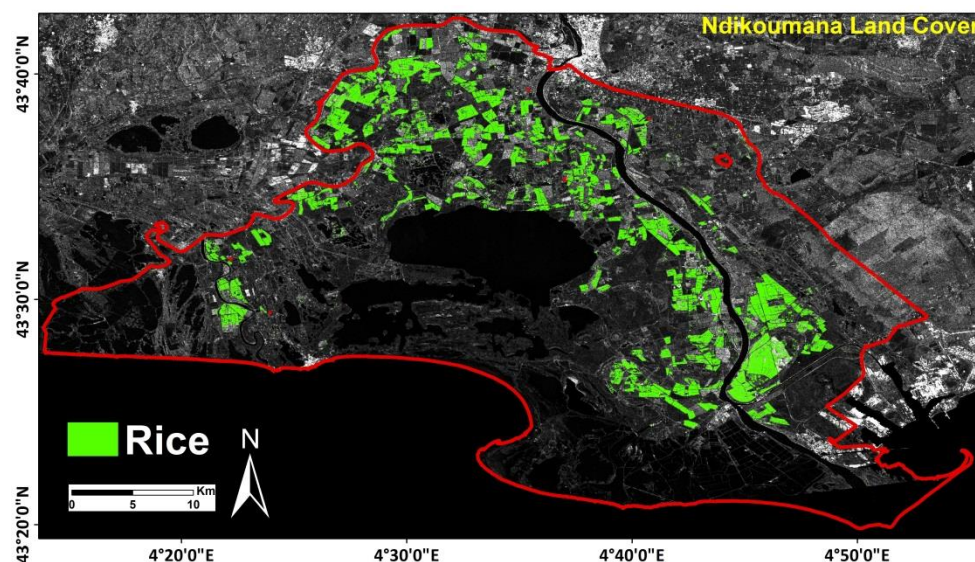


Figure 10. Rice areas in Camargue in 2017 extracted from Ndikumana et al. [25] land cover map. The background is a SAR image in VV polarization.

Table 4. Confusion matrix for the comparison between rice areas derived from Ndikumana Agricultural Land Cover and rice areas from RPG-2017 data.

Class Value	Rice	Other Crop	Total	User Accuracy
Rice	3042	403	3445	88.3%
Other Crop	153	6369	6522	97.6%
Total	3159	6772	9967	
Producer Accuracy	95.2%	94.0%		
Overall Accuracy			94.4%	
Kappa			87.5%	
F ₁ score			91.6%	

Several studies have already used traditional machine learning algorithms for paddy rice mapping such as RF, Support Vector Machine (SVM), and decision tree [24,30–34]. Recently, Zhang et al. [31] used the Land Surface Temperature and phenological parameters derived from the NDVI time series of Landsat 8 images (fused with MODIS NDVI to overcome the cloud limitation) with a convolutional neural network approach to map rice areas in the Dongting Lake Area of China. The overall accuracy obtained was 97.1%. On the other hand, when using the classical machine learning methods (SVM and RF) their accuracy decreased to 90.6% and 89.4%, respectively. They report in their study that rice and other crops are often misclassified when using only the spectral information of optical images. When the spectral features were only considered, rice plots were misclassified as grassland and other vegetation type. This limitation is not present in our study as we were able to accurately classify rice areas in the presence of other crops especially those grown in summer (sunflower, grassland ...). In addition, Mansaray et al. [30] combined the VH polarization of Sentinel-1A images with NDVI and Modified NDWI derived from Landsat-8 images to map rice areas in southeast China. Using the decision tree approach, they reached an overall accuracy of 85% when using both SAR and Optical data. Using only S1A images the overall accuracy obtained in their study was 79%. The study site examined was mainly composed of urban, water, and tree areas. Moreover, the data fusion of optical and radar time series has been also performed in the study of Park et al. [32] where they mapped rice areas by combining Landsat-8 images with SAR data of RADARSAT and ALOS/PALSAR on two sites in South Korea. The highest accuracy (98.7%) was obtained when using a fusion of SAR and optical data with a digital elevation model and applying the SVM classification. The land cover in the studied zone was mainly composed of rice, grains, pasture, bare soil and vineyards. A common limitation among these discussed studies is the cloud cover that limits the availability of optical images during the rice growing cycle. Using only SAR data, Zhang et al. [33] mapped paddy rice using multi-temporal ALOS/PALSAR imagery in southeast China. The studied area was mainly composed of rice, dryland crops (e.g., rapeseed, vegetables) and orchards. They obtained 90% user accuracy and 76% producer accuracy when applying the SVM classifier. Lasko et al. [24] have mapped rice areas using Sentinel-1A time series in Hanoi, Vietnam by applying the random forest classifier. The highest overall accuracy (93.3%) was obtained when using the VV/VH ratio. Clauss et al. [34] also mapped rice areas over six different study sites using S1 temporal series by applying the decision tree. They chose the VH polarization due to the high dynamic range of backscatter over rice areas. They achieved an overall accuracy of 83%. In their study they recommend that increasing the temporal density of the used Sentinel-1 images would help better increase the accuracy of the classification.

Most studies tend to use classical machine learning methods applied on optical or/and SAR data in order to map rice areas. Among the several discussed studies, our proposed method remains powerful since it combines the high accuracy, the simplicity of the applied method and the availability of the used dataset. The obtained accuracy is equivalent and even better than accuracies obtained by complex methods that may require large input datasets. Although the supervised classification highly depends on the study site (mainly on existing crop types) and ground data, the proposed approach could be

used in any agricultural area with similar rice cropping practices and land cover. However, the metrics and the threshold used in this study should be adapted for a good application of this method in other geographical contexts. The method uses the SAR temporal signature of rice plots during its growing season to classify the rice areas. The temporal behavior of the SAR backscattering for rice plots allows us to extract metrics that best describe the rice cultivation, regardless of the surrounding agricultural land cover. Thus, the suggested classification could be applied over different study sites. Moreover, unlike other approaches that directly implement the entire time series to classify a crop type, this method concentrates on first describing a rice cultivation using the SAR time series and introducing relevant metrics that allow us to accurately detect rice crops in a classification technique. Future work should concentrate on the implementation of this approach over other study sites to ensure the transferability of the method. The method could be adapted to other study sites with other forms of land cover and crop types. Moreover, it could be adjusted to work over sites with more than one cropping cycle of rice per year.

6. Conclusions

In this paper, a simple yet powerful tool for mapping the rice area over the Camargue region of France using a Sentinel-1 SAR data time series was introduced. The SAR backscattering time series of 11 agricultural crop types in the area were first analyzed during the period between May 2017 and September 2017. The analysis of the SAR temporal behavior revealed that rice crops are clearly described by Gaussian profile of the “VV/VH” time series, an increasing linear profile of the “VH” time series, and a high fluctuation in the VV/VH signal when compared to other crop types. To classify rice areas using this description, the position of the maximum, standard deviation, and correlation coefficient of the Gaussian fitting curve of VV/VH, the variance of the VV/VH signal, and the slope of the linear fitting of the VH signal were extracted for each plot during the period between May 2017 and September 2017. The derived metrics were then introduced into a decisional tree and a random forest classifier to classify the rice areas. The results show a significant accuracy when comparing the classified rice map to the national data. A very high overall accuracy was obtained using both the decisional tree (96.3%) and RF classifier (96.6%). Finally, the accuracy of the estimated rice area reaches 97.3% when comparing the rice classified area to the declared rice area for the year 2017.

Author Contributions: H.B. (Hassan Bazzi) and N.B. conceived and designed the experiments; H.B. (Hassan Bazzi) and M.E.H. performed the experiments; H.B. (Hassan Bazzi), N.B., and M.E.H., analyzed the results; H.B. (Hassan Bazzi) wrote the article; M.Z., D.H.T.M., E.N., D.C., and H.B. (Hatem Belhouchette) revised the paper.

Funding: This research received funding from the French Space Study Center (CNES, TOSCA 2018 project, POMME-V), the National Research Institute of Science and Technology for Environment and Agriculture (IRSTEA), and the European Space Agency (ESA).

Acknowledgments: The authors wish to thank the French Space Study Center (2018 TOSCA) and the National Research Institute of Science and Technology for Environment and Agriculture (IRSTEA) for supporting this work. The authors also wish to thank Laure Hossard of the National Institute of Agricultural Research (INRA) for providing the terrain reference data, providing vector map on Camargue area, land use ground data, and contacts to farmers.

Conflicts of Interest: The authors declare no conflict of interest.

References

1. FAO. FAO Rice Market Monitor. 2018, Volume XXI. Available online: <http://www.fao.org/3/I9243EN/i9243en.pdf> (accessed on 28 March 2019).
2. Delmotte, S.; Tittone, P.; Mouret, J.-C.; Hammond, R.; Lopez-Ridaura, S. On farm assessment of rice yield variability and productivity gaps between organic and conventional cropping systems under Mediterranean climate. *Eur. J. Agron.* **2011**, *35*, 223–236. [CrossRef]
3. El Hajj, M.; Baghdadi, N.; Zribi, M.; Belaud, G.; Cheviron, B.; Courault, D.; Charron, F. Soil moisture retrieval over irrigated grassland using X-band SAR data. *Remote Sens. Environ.* **2016**, *176*, 202–218. [CrossRef]

4. El Hajj, M.; Baghdadi, N.; Zribi, M.; Bazzi, H. Synergic Use of Sentinel-1 and Sentinel-2 Images for Operational Soil Moisture Mapping at High Spatial Resolution over Agricultural Areas. *Remote Sens.* **2017**, *9*, 1292. [[CrossRef](#)]
5. Gao, Q.; Zribi, M.; Escorihuela, M.; Baghdadi, N.; Segui, P. Irrigation Mapping Using Sentinel-1 Time Series at Field Scale. *Remote Sens.* **2018**, *10*, 1495. [[CrossRef](#)]
6. Nasrallah, A.; Baghdadi, N.; Mhawej, M.; Faour, G.; Darwish, T.; Belhouchette, H.; Darwich, S. A Novel Approach for Mapping Wheat Areas Using High Resolution Sentinel-2 Images. *Sensors* **2018**, *18*, 2089. [[CrossRef](#)] [[PubMed](#)]
7. Aubert, M.; Baghdadi, N.N.; Zribi, M.; Ose, K.; El Hajj, M.; Vaudour, E.; Gonzalez-Sosa, E. Toward an Operational Bare Soil Moisture Mapping Using TerraSAR-X Data Acquired Over Agricultural Areas. *IEEE J. Sel. Top. Appl. Earth Obs. Remote Sens.* **2013**, *6*, 900–916. [[CrossRef](#)]
8. Baghdadi, N.N.; El Hajj, M.; Zribi, M.; Fayad, I. Coupling SAR C-Band and Optical Data for Soil Moisture and Leaf Area Index Retrieval Over Irrigated Grasslands. *IEEE J. Sel. Top. Appl. Earth Obs. Remote Sens.* **2016**, *9*, 1229–1243. [[CrossRef](#)]
9. Xiao, X.; Boles, S.; Liu, J.; Zhuang, D.; Frohling, S.; Li, C.; Salas, W.; Moore, B. Mapping paddy rice agriculture in southern China using multi-temporal MODIS images. *Remote Sens. Environ.* **2005**, *95*, 480–492. [[CrossRef](#)]
10. Son, N.-T.; Chen, C.-F.; Chen, C.-R.; Duc, H.-N.; Chang, L.-Y. A Phenology-Based Classification of Time-Series MODIS Data for Rice Crop Monitoring in Mekong Delta, Vietnam. *Remote Sens.* **2013**, *6*, 135–156. [[CrossRef](#)]
11. Sakamoto, T.; Sprague, D.S.; Okamoto, K.; Ishitsuka, N. Semi-automatic classification method for mapping the rice-planted areas of Japan using multi-temporal Landsat images. *Remote Sens. Appl. Soc. Environ.* **2018**, *10*, 7–17. [[CrossRef](#)]
12. Zhang, X.; Wu, B.; Ponce-Campos, G.; Zhang, M.; Chang, S.; Tian, F. Mapping up-to-Date Paddy Rice Extent at 10 M Resolution in China through the Integration of Optical and Synthetic Aperture Radar Images. *Remote Sens.* **2018**, *10*, 1200. [[CrossRef](#)]
13. Clauss, K.; Yan, H.; Kuenzer, C. Mapping Paddy Rice in China in 2002, 2005, 2010 and 2014 with MODIS Time Series. *Remote Sens.* **2016**, *8*, 434. [[CrossRef](#)]
14. Li, P.; Xiao, C.; Feng, Z. Mapping Rice Planted Area Using a New Normalized EVI and SAVI (NVI) Derived from Landsat-8 OLI. *IEEE Geosci. Remote Sens. Lett.* **2018**, *99*, 1–5. [[CrossRef](#)]
15. Wang, L.-F.; Kong, J.A.; Ding, K.H.; Le Toan, T.; Ribbes, F.; Floury, N. Electromagnetic scattering model for rice canopy based on monte carlo simulation. *Prog. Electromagn. Res.* **2005**, *52*, 153–171. [[CrossRef](#)]
16. Bouvet, A.; Le Toan, T. Use of ENVISAT/ASAR wide-swath data for timely rice fields mapping in the Mekong River Delta. *Remote Sens. Environ.* **2011**, *115*, 1090–1101. [[CrossRef](#)]
17. Nguyen, D.; Clauss, K.; Cao, S.; Naeimi, V.; Kuenzer, C.; Wagner, W. Mapping Rice Seasonality in the Mekong Delta with Multi-Year Envisat ASAR WSM Data. *Remote Sens.* **2015**, *7*, 15868–15893. [[CrossRef](#)]
18. Lopez-Sanchez, J.M.; Ballester-Berman, J.D.; Hajnsek, I. First Results of Rice Monitoring Practices in Spain by Means of Time Series of TerraSAR-X Dual-Pol Images. *IEEE J. Sel. Top. Appl. Earth Obs. Remote Sens.* **2011**, *4*, 412–422. [[CrossRef](#)]
19. Shao, Y.; Fan, X.; Liu, H.; Xiao, J.; Ross, S.; Brisco, B.; Brown, R.; Staples, G. Rice monitoring and production estimation using multitemporal RADARSAT. *Remote Sens. Environ.* **2001**, *76*, 310–325. [[CrossRef](#)]
20. Nelson, A.; Setiyono, T.; Rala, A.; Quicho, E.; Raviz, J.; Abonete, P.; Maunahan, A.; Garcia, C.; Bhatti, H.; Villano, L.; et al. Towards an Operational SAR-Based Rice Monitoring System in Asia: Examples from 13 Demonstration Sites across Asia in the RIICE Project. *Remote Sens.* **2014**, *6*, 10773–10812. [[CrossRef](#)]
21. Nguyen, D.B.; Gruber, A.; Wagner, W. Mapping rice extent and cropping scheme in the Mekong Delta using Sentinel-1A data. *Remote Sens. Lett.* **2016**, *7*, 1209–1218. [[CrossRef](#)]
22. Clauss, K.; Ottinger, M.; Leinenkugel, P.; Kuenzer, C. Estimating rice production in the Mekong Delta, Vietnam, utilizing time series of Sentinel-1 SAR data. *Int. J. Appl. Earth Obs. Geoinf.* **2018**, *73*, 574–585. [[CrossRef](#)]
23. Forino, G.; Nunziata, F.; Mascolo, L.; Pugliano, G.; Migliaccio, M. Rice Mapping and Sowing Date Estimation Using CSK SAR Data. In Proceedings of the 2018 IEEE 4th International Forum on Research and Technology for Society and Industry (RTSI), Palermo, Italy, 10–13 September 2018; pp. 1–4.
24. Lasko, K.; Vadrevu, K.P.; Tran, V.T.; Justice, C. Mapping Double and Single Crop Paddy Rice with Sentinel-1A at Varying Spatial Scales and Polarizations in Hanoi, Vietnam. *IEEE J. Sel. Top. Appl. Earth Obs. Remote Sens.* **2018**, *11*, 498–512. [[CrossRef](#)]

25. Ndikumana, E.; Ho Tong Minh, D.; Baghdadi, N.; Courault, D.; Hossard, L. Deep Recurrent Neural Network for Agricultural Classification using multitemporal SAR Sentinel-1 for Camargue, France. *Remote Sens.* **2018**, *10*, 1217. [[CrossRef](#)]
26. Schwerdt, M.; Schmidt, K.; Tous Ramon, N.; Klenk, P.; Yague-Martinez, N.; Prats-Iraola, P.; Zink, M.; Geudtner, D. Independent System Calibration of Sentinel-1B. *Remote Sens.* **2017**, *9*, 511. [[CrossRef](#)]
27. Quegan, S.; Yu, J.J. Filtering of multichannel SAR images. *IEEE Trans. Geosci. Remote Sens.* **2001**, *39*, 2373–2379. [[CrossRef](#)]
28. Landis, J.R.; Koch, G.G. The measurement of observer agreement for categorical data. *Biometrics* **1977**, *33*, 159–174. [[CrossRef](#)]
29. Fawcett, T. An introduction to ROC analysis. *Pattern Recognit. Lett.* **2006**, *27*, 861–874. [[CrossRef](#)]
30. Mansaray, L.; Huang, W.; Zhang, D.; Huang, J.; Li, J. Mapping Rice Fields in Urban Shanghai, Southeast China, Using Sentinel-1A and Landsat 8 Datasets. *Remote Sens.* **2017**, *9*, 257. [[CrossRef](#)]
31. Zhang, M.; Lin, H.; Wang, G.; Sun, H.; Fu, J. Mapping Paddy Rice Using a Convolutional Neural Network (CNN) with Landsat 8 Datasets in the Dongting Lake Area, China. *Remote Sens.* **2018**, *10*, 1840. [[CrossRef](#)]
32. Park, S.; Im, J.; Park, S.; Yoo, C.; Han, H.; Rhee, J. Classification and Mapping of Paddy Rice by Combining Landsat and SAR Time Series Data. *Remote Sens.* **2018**, *10*, 447. [[CrossRef](#)]
33. Zhang, Y.; Wang, C.; Wu, J.; Qi, J.; Salas, W.A. Mapping paddy rice with multitemporal ALOS/PALSAR imagery in southeast China. *Int. J. Remote Sens.* **2009**, *30*, 6301–6315. [[CrossRef](#)]
34. Clauss, K.; Ottinger, M.; Kuenzer, C. Mapping rice areas with Sentinel-1 time series and superpixel segmentation. *Int. J. Remote Sens.* **2018**, *39*, 1399–1420. [[CrossRef](#)]



© 2019 by the authors. Licensee MDPI, Basel, Switzerland. This article is an open access article distributed under the terms and conditions of the Creative Commons Attribution (CC BY) license (<http://creativecommons.org/licenses/by/4.0/>).